RANS-SMC AND HYBRID LES/RANS MODELLING OF A BACKWARD-FACING STEP FLOW SUBJECTED TO INCREASINGLY ENHANCED WALL HEATING

Björn Kniesner, Roland Jester-Zürker and Suad Jakirlić
Fachgebiet Strömungslehre und Aerodynamik, Technische Universität Darmstadt
Petersenstr. 30, D-64287 Darmstadt, Germany
b.kniesner@sla.tu-darmstadt.de, roland.jester-zuerker@voith.com, s.jakirlic@sla.tu-darmstadt.de

Kemal Hanjalić
Marie Curie Chair, Dipartimento di Meccanica ed Aeronautica, Università di Roma 'La Sapienza'
Via Eudossiana 18, 00184 Roma, Italy
hanjalic@dma.ing.uniroma1.it

ABSTRACT

Turbulent flow over a backward-facing step (Re_H = 5540; $ER = 1.5$) subjected to large temperature gradients originating from an increasingly enhanced heat flux through the step wall is investigated computationally by using a near-wall Second-Moment Closure model (SMC) in the RANS (Reynolds-averaged Navier-Stokes) framework and a hybrid LES/RANS (HLR) scheme. Reference Large Eddy Simulations (LES) were performed by Avancha and Pletcher (2002). Corresponding isothermal flow was investigated experimentally by Kasagi and Matsunaga (1995). The results obtained by present simulations follow closely the reference database, especially for the mean velocity evolution and the bulk and wall temperature variations. An important outcome of the present study is a substantial increase of the friction coefficient with the increase in the wall heating both in the flow reversal and recovery region, associated with the local flow acceleration in the immediate wall vicinity.

INTRODUCTION

Turbulent flow over a backward-facing step is one of the most frequently encountered flow configurations in technical practice. A large number of relevant experimental and computational studies can be found in the open literature. Despite its geometrical simplicity, this flow exhibits a number of interesting features, and has served as a popular test case for studying flow separation, reattachment and recovery as well as the influence of the local streamline curvature and adverse pressure gradient. The flow separates at the step edge, forming a highly unsteady, curved shear layer which impinges and bifurcates at the reattachment region; one branch flowing back creates mean and secondary recirculation zones behind the step, another branch creates a new boundary layer downstream. Unlike the flows separated from continuous surfaces characterized by highly intermittent separation region whose oscillations spread over a substantial portion of the flow, the backward-facing step flow, characterized by a fixed separation point, can be well solved by an advanced RANS model. The important prerequisite for succesful computation of the flow in the whole is the accurate capturing of the near-wall turbulence, characterized by strong Reynolds-stress and stress-dissipation anisotropy. The deviation from equilibrium conditions in this flow region is further enhanced by strong temperature gradients (encountered e.g. in gas combustors, heat exchangers, etc.). The influence of strong heating is primarily manifested through a severe variation of the fluid properties (density, viscosity) leading consequently to significant structural changes in the turbulence field. The strongest modification of the flow structure occurs in the inner part of the temperature layer.

The main goal of this work is to validate a low-Reynolds-number turbulence model based on the solution of transport equations for the turbulent stress tensor and heat flux vector, and a two-layer hybrid LES/RANS method coupling a near-wall $k-\varepsilon$ RANS model with an LES in the outer layer, both in separated flows with strong property variations due to intensive heating.

FLOW DESCRIPTION

Schematic of the flow configuration indicating the domain of interest is displayed in Fig. 1. The flow Reynolds number based on the step height and the upstream centerline velocity is $Re_H = 5540$ ($H = 0.041m$). The upstream conditions correspond to fully-developed flow in a channel of height $h = 2H$ (inflow was generated by performing precursor channel flow calculations) providing the expansion ratio of $ER = 1.5$. The bottom wall downstream of the step was heated by a uniformly supplied heat flux, the latter representing the thermal boundary conditions. Three cases with increasing heat flux (q_w = 1, 2 and 3 kW/m^2; reference LES by Avancha and Pletcher, 2002) were computed in addition to the isothermal flow (Exp.: Kasagi and Matsunaga, 1995). All other flow and fluid properties were adopted from the work of Avancha and Pletcher: $U = 2.063\,m/s$, $T_{ref} = 293\,K$, $\varrho_{ref} = 1.194\,kg/m^3$, $\lambda_{ref} = 0.2574\,W/(mK)$, $\nu_{ref} = \mu_{ref}/\varrho_{ref} = 1.527 \times 10^{-5} m^2/s$, $Pr = 0.71$ and $C_p = 1006\,J/(kgK)$.

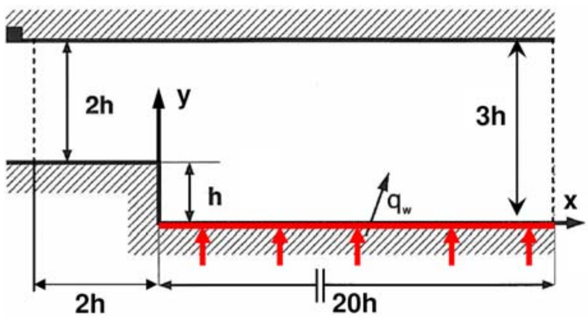

Figure 1: Schematic of flow configuration considered

COMPUTATIONAL MODEL

The continuity ($\partial\overline{\varrho}/\partial t + \partial(\overline{\varrho}\widetilde{U}_i)/\partial x_i = 0$), momentum and energy equations governing the flow and heat transfer under the variable property conditions read:

$$\frac{\partial\left(\overline{\varrho}\widetilde{U}_i\right)}{\partial t} + \frac{\partial\left(\overline{\varrho}\widetilde{U}_j\widetilde{U}_i\right)}{\partial x_j} = -\frac{\partial\overline{P}}{\partial x_i} + \frac{\partial}{\partial x_j}\left(\overline{\tau}^{\mu}_{ij} + \overline{\tau}^{t}_{ij}\right) \quad (1)$$

$$\frac{\partial\left(\overline{\varrho}C_p\widetilde{T}\right)}{\partial t} + \frac{\partial\left(\overline{\varrho}C_p\widetilde{U}_j\widetilde{T}\right)}{\partial x_j} = \frac{\partial}{\partial x_j}\left(\overline{q}^{\mu}_j + \overline{q}^{t}_j\right) \quad (2)$$

Here, $\overline{\tau}^{\mu}_{ij}$ ($= 2\overline{\mu}\widetilde{S}_{ij} - 2\overline{\mu}\widetilde{S}_{kk}\delta_{ij}/3$; $\widetilde{S}_{ij} = 0.5(\partial\widetilde{U}_i/\partial x_j + \partial\widetilde{U}_j/\partial x_i)$) and $\overline{q}^{\mu}_j$ ($= \overline{\lambda}\partial\widetilde{T}/\partial x_j$; with $\overline{\lambda} = C_p\overline{\mu}/Pr$) represent viscous stress tensor and viscous heat flux, whereas turbulent stress tensor $\overline{\tau}^{t}_{ij}$ and turbulent heat flux $\overline{q}^{t}_j$ are to be modelled (see the following subsections). It is noted, that the term $\overline{\tau}^{\mu}_{ij}\widetilde{S}_{ij}$ denoting the (viscous) dissipation function is omitted in the energy equation. Its contribution is negligible at low Mach numbers applied in the present work. In these equations the overbar ($\overline{\Phi}$) and the tilde ($\widetilde{\Phi}$) denote the standard (Reynolds) and the mass weighted (Favre) averages ($\widetilde{\Phi} \equiv \overline{\varrho\Phi}/\overline{\varrho}$), respectively. The temperature dependence on viscosity μ and heat conductivity λ is defined via a power-law formulation, while Prandtl number Pr and specific heat at constant pressure C_p were kept constant.

$$\overline{\mu} = \mu_{ref}\left(\widetilde{T}/T_{ref}\right)^{0.71}; \quad \overline{\lambda} = \lambda_{ref}\left(\widetilde{T}/T_{ref}\right)^{0.71} \quad (3)$$

Density is evaluated from the equation for ideal gas $\overline{\varrho} = \overline{P}/(R\widetilde{T})$, with R denoting the universal gas constant.

The most important features of the two turbulence models used in this work are outlined in the next two subsections. For detailed specification of both models, readers are referred to Jakirlic and Hanjalic (2002), Jester-Zürker and Jakirlic (2005) and Kniesner et al. (2006).

Near-wall, Second-Moment Closure Model

The present model implies the solution of modelled transport equation for the Reynolds stress tensor $\widetilde{u''_i u''_j}$ ($\overline{\tau}^{t}_{ij} = -\overline{\varrho}\widetilde{u''_i u''_j}$ in Eq. 1) and the equation governing a new scale-providing variable, referred to as the 'homogeneous dissipation rate' ε^h (Fig. 2), Jakirlic and Hanjalic (2002):

$$\frac{\partial(\overline{\varrho}\widetilde{U}_k\widetilde{u''_i u''_j})}{\partial x_k} = \frac{1}{2}\mathcal{D}^{\nu}_{ij} + \mathcal{D}^{t}_{ij} + \overline{\varrho}(\mathcal{P}_{ij} - \varepsilon^h_{ij} + \Phi_{ij} + \Phi^{w}_{ij}) \quad (4)$$

$$\frac{\partial(\overline{\varrho}\widetilde{U}_k\varepsilon^h)}{\partial x_k} = \frac{1}{2}\mathcal{D}^{\nu}_{\varepsilon} + \mathcal{D}^{t}_{\varepsilon} + \overline{\varrho}(C_{\varepsilon,1}\mathcal{P}_k - C_{\varepsilon,2}f_\varepsilon\tilde{\varepsilon}^h)\frac{\varepsilon^h}{k} + C_{\varepsilon,3}\overline{\mu}\frac{k}{\varepsilon^h}\widetilde{u''_j u''_k}\frac{\partial^2\widetilde{U}_i}{\partial x_j\partial x_l}\frac{\partial^2\widetilde{U}_i}{\partial x_k\partial x_l} \quad (5)$$

The main features of the model are an anisotropic formulation of the dissipation correlation ε^h_{ij}, a quadratic formulation of the pressure strain model term Φ_{ij} and a wall-normal-free formulation of the Gibson and Launder (1978) wall reflection term Φ^{w}_{ij}. The model of turbulent diffusion $\mathcal{D}^{t}_{ij}$ is that of Daly and Harlow (1970). The quantity ε^h differs from the conventional dissipation rate ε ($= \varepsilon^h + 0.5\mathcal{D}^{\nu}_k$) by a non-homogeneous part, which is active only in the immediate wall vicinity up to $y^+ \approx 20$. This "inhomogeneous" part corresponds exactly to one half of the molecular diffusion of the kinetic energy of turbulence ($0.5\mathcal{D}^{\nu}_k$, see Fig. 2) and, thus, it needs no modelling. Such an approach offers a number of convenient advantages: the dissipation equation (5) retains the same basic form, the proper near-wall behaviour of ε is recovered without any additional terms, and the correct asymptotic behaviour of the stress dissipation components $\varepsilon_{ij} = \varepsilon^h_{ij} + \mathcal{D}^{\nu}_{ij}/2$ when a solid wall is approached is fulfilled automatically without necessity for any wall geometry-related parameter. The applied turbulence model for the variable fluid property (i.e. compressible) cases is a straight-forward adaptation of the incompressible version of the turbulence model.

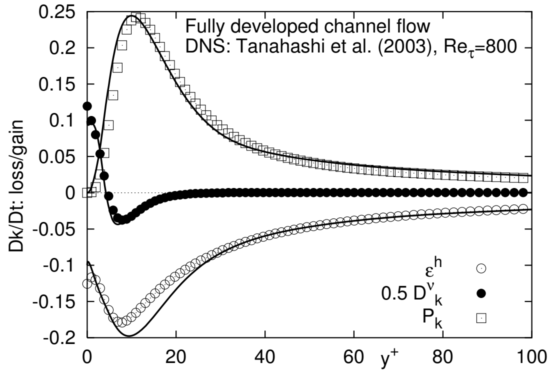

Figure 2: Terms in the budget of the equation for the kinetic energy of turbulence in a channel flow with constant fluid properties obtained with the present turbulence model

The turbulent heat flux $\overline{q}^t_i = -\overline{\varrho}C_p\widetilde{u''_i\theta}$ appearing in Eq. (2) is computed also at the second-moment level by solving the modelled differential equation in conjunction with the differential near-wall, Reynolds-stress model described above:

$$\frac{D(\overline{\varrho}\widetilde{u''_i\theta})}{Dt} = \mathcal{D}^{\nu}_{i\theta} + \mathcal{D}^{t}_{i\theta} + \overline{\varrho}\mathcal{P}_{i\theta} + \overline{\varrho}\Phi_{i\theta} - \overline{\varrho}\varepsilon_{i\theta} \quad (6)$$

The model formulation of the pressure-temperature gradient term $\overline{\varrho}\Phi_{i\theta}$ accounting for contributions from both the mean velocity and the mean scalar gradients applied in this work represents a recent development of Seki et al. (2003). The model for the turbulent transport $\mathcal{D}^{t}_{i\theta}$ is the gradient diffusion model due to Daly and Harlow (1970). The viscous dissipation model adopted in the present work is the proposal of Lai and So (1990).

Numerical method. All computations were performed by an own in-house computer code based on the Finite Volume numerical method (2nd order) for solving RANS-equations in the orthogonal coordinate system. The closest-to-the-wall grid point was located at $y^+ \leq 0.5$. In order to account for the compressibility effects an appropriately modified SIMPLE pressure-correction method in conjunction with the collocated variable arrangement was used.

Hybrid LES/RANS Model

In the present hybrid LES/RANS formulation, the RANS model covers the near-wall region and the LES model the remainder of the flow domain. Both methods share the same temporal resolution. The mass-weighted equations governing the velocity (Eq. 1) and temperature (Eq. 2) fields operate as the Reynolds-averaged Navier-Stokes equations in the near-wall layer ($\widetilde{U}_i$ and $\widetilde{T}$ represent the mass-weighted, ensemble-averaged velocity and temperature fields U_i and T) or as the filtered Navier-Stokes equations in the outer layer ($\widetilde{U}_i$ and $\widetilde{T}$ represent the mass-weighted, spatially filtered velocity and temperature fields). The turbulent stress tensor $\overline{\tau}^t_{ij}$ in Eq. (1) representing either the subgrid-stress tensor or the Reynolds-stress tensor is expressed in terms of the mean strain tensor $\widetilde{S}_{ij}$ via the Boussinesq relationship:

$$\overline{\tau}^t_{ij} = \overline{\mu}_t \left(\frac{\partial \widetilde{U}_i}{\partial x_j} + \frac{\partial \widetilde{U}_j}{\partial x_i} - \frac{2}{3}\frac{\partial \widetilde{U}_k}{\partial x_k}\delta_{ij} \right) \tag{7}$$

The turbulent heat flux $\overline{q}^t_i$ in the equation governing the temperature field is modelled by using the simple gradient diffusion hypothesis

$$\overline{q}^t_i = -\overline{\varrho} C_p \widetilde{u_i \theta} = \overline{\lambda}_t \frac{\partial \widetilde{T}}{\partial x_i} \text{ with } \overline{\lambda}_t = \frac{\overline{\mu}_t C_p}{Pr_t} \tag{8}$$

The equations governing the velocity and temperature field in the hybrid LES/RANS framework are:

$$\frac{\mathbf{D}(\overline{\rho}\tilde{U}_i)}{\mathbf{D}t} = -\frac{\partial \overline{p}^*}{\partial x_i} + \frac{\partial}{\partial x_j}\left[(\overline{\mu} + \overline{\mu}_t)\left(\frac{\partial \tilde{U}_i}{\partial x_j} + \frac{\partial \tilde{U}_j}{\partial x_i} - \frac{2}{3}\frac{\partial \tilde{U}_k}{\partial x_k}\delta_{ij} \right)\right] \tag{9}$$

$$\frac{\mathbf{D}(\overline{\rho}\tilde{T})}{\mathbf{D}t} = \frac{\partial}{\partial x_j}\left[\left(\frac{\overline{\mu}}{Pr} + \frac{\overline{\mu}_t}{Pr_t} \right)\left(\frac{\partial \tilde{T}}{\partial x_j} \right)\right] \tag{10}$$

In the present two layer hybrid LES/RANS scheme the coupling of the instantaneous LES field and the ensemble-averaged RANS field at the interface is realized via the turbulent viscosity, which makes it possible to obtain solutions using one system of equations. This means practically that the governing equations (9) and (10) are solved in the entire solution domain irrespective of the flow sub-region (LES or RANS). Depending on the flow zone, the hybrid model implies the determination of the turbulent viscosity $\overline{\mu}_t$ either from a $k-\varepsilon$ RANS model: $\overline{\mu}_t = \overline{\varrho} C_\mu f_\mu k^2/\varepsilon$ or from the LES formulation: $\overline{\mu}_t = \overline{\mu}_{SGS} = \overline{\varrho}(C_S \Delta)^2 |\widetilde{S}|$. The Smagorinsky constant C_S takes the value of 0.1. $\Delta = (\Delta x \times \Delta y \times \Delta z)^{1/3}$ represents the filter width and $|\widetilde{S}| = (\widetilde{S}_{ij}\widetilde{S}_{ij})^{1/2}$ the strain rate modulus.

The near-wall variation of the turbulent viscosity $\overline{\mu}_t$ is obtained from a $k - \varepsilon$ RANS model implying solving of the following two transport equations:

$$\frac{\mathbf{D}(\overline{\varrho}\tilde{k})}{\mathbf{D}t} = \frac{\partial}{\partial x_j}\left[\left(\overline{\mu} + \frac{\overline{\mu}_t}{\sigma_k} \right) \frac{\partial k}{\partial x_j} \right] + \overline{\varrho}\mathcal{P}_k - \overline{\varrho}\varepsilon \tag{11}$$

$$\frac{\mathbf{D}(\overline{\varrho}\varepsilon)}{\mathbf{D}t} = \frac{\partial}{\partial x_j}\left[\left(\overline{\mu} + \frac{\overline{\mu}_t}{\sigma_\varepsilon} \right) \frac{\partial \varepsilon}{\partial x_j} \right] + \overline{\varrho}\frac{C_{\varepsilon,1}\mathcal{P}_k - f_\varepsilon C_{\varepsilon,2}\varepsilon}{\tau} + \mathcal{P}_{\varepsilon,3} \tag{12}$$

with $\tau = k/\varepsilon$. The near-wall and viscous damping functions (f_μ and f_ε) and the production term $\mathcal{P}_{\varepsilon,3}$ (Eqs. 11 and 12), are presently modelled in line with the proposal of Chien (1982) with ε representing the isotropic part of the total viscous dissipation rate taking zero value at the wall.

Because k and ε are not provided (in the case of the subgrid-scale (SGS) model of Smagorinsky) within the LES sub-domain, their SGS values are estimated using the proposal of Mason and Callen (1986):

$$k_{SGS} = \frac{(C_S\Delta)^2 |\widetilde{S}|^2}{0.3} \text{ and } \varepsilon_{SGS} = (C_S\Delta)^2|\widetilde{S}|^3 \tag{13}$$

The RANS equations for k and ε are solved in the entire flow field, but with the discretization coefficients taking zero values in the LES sub-region. By manipulating appropriately the source terms, the numerical solution of these equations in the framework of the finite volume method provides the interface values of the k_{RANS} and ε_{RANS} being equal to the corresponding SGS values. By doing so, the boundary condition at the LES/RANS interface (*ifce*) implying the equality of the modelled turbulent viscosities (by assuming the continuity of their resolved contributions across the interface, Temmerman et al., 2005) at both sides of the interface:

$$\overline{\mu}_{t,ifce}|_{RANS-side} = \overline{\mu}_{t,ifce}|_{LES-side}$$

is implicitly imposed without any further adjustment, see Fig. 3 for illustration. In such a way a smooth transition of the turbulent viscosity is ensured.

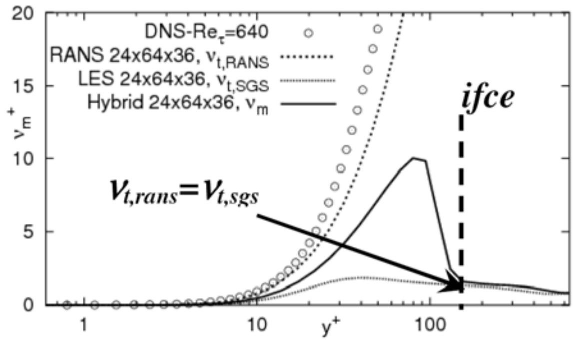

Figure 3: Variation of modelled turbulent viscosity across the interface in a fully-developed channel flow

One of the advantages of a zonal approach is the possibility to predefine the LES-RANS interface. However, in unknown flow configurations, this could be a difficult issue. Therefore, a certain criteria expressed in terms of a control parameter should be introduced. Presently, the following control parameter

$$k^* = \left\langle \frac{k_{mod}}{k_{mod} + k_{res}} \right\rangle \tag{14}$$

is adopted, representing the ratio of the modelled (SGS) to the total turbulent kinetic energy in the LES region, averaged over all grid cells in homogeneous direction at the interface on the LES side. As soon as this value exceeds 20 %, the interface is moved farther from the wall and in opposite direction when the value goes below 20 %. This additionally ensures that in the limit of a very fine grid (very low level of the residual turbulence) LES is performed in the most of the solution domain. In contrast, in the case of a coarse grid, RANS prevails. As the interface separates the near wall region from the reminder of the flow, it would be suitable to choose a wall-defined parameter for denoting the interface location. In the present study, the dimensionless wall distance y^+ was adopted. Despite possible difficulties in respect to the definition of y^+ in flow domains where the wall shear stress approaches zero, as e.g. in separation and reattachment regions, no problems in the course of the computations have arisen (one may recall that the same non-dimensional wall distance y^+ is regularly used in the Van Driest's wall-damping of μ_t also in LES of separating and reattaching flows). It is noted, that the interface y^+ doesn't represent a model parameter in the HLR method. It only denotes the computational nodes at which the prescribed value of k^* is obtained. Fig. 4 displays a snapshot of the instantaneous velocity field with the corresponding evolution of the averaged interface value along the upper wall and the lower (step) wall.

Numerical method. All computations were performed with the in-house computer code FASTEST based on a

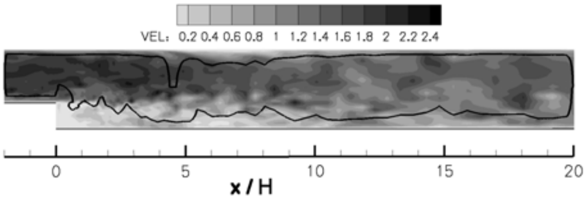

Figure 4: Instantaneous velocity field and the corresponding evolution of the interface value $y^+_{ifce} = 48$

finite volume numerical method for solving both the three-dimensional filtered and Reynolds-averaged Navier-Stokes equations on block structured, body fitted, non-orthogonal meshes. Block interfaces are treated in a conservative manner, consistent with the treatment of the inner cell faces. A cell centered (collocated) variable arrangement and Cartesian vector and tensor components are used. The well-known SIMPLE algorithm is applied for coupling the velocity and pressure fields. The convective terms in all equations are discretized by a second-order central differencing scheme, whose stability is enhanced by the deferred correction approach (see e.g., Khosla and Rubin, 1974). The time discretization is accomplished applying the second order (implicit) Crank-Nicolson method.

The grid covering the flow domain after expansion (20 step heights, Fig. 1) contains $72 \times 42 \times 40$ cells. The inflow plane was positioned at two step heights upstream from the step edge. This inlet region was meshed with additional $14 \times 28 \times 40$ grid cells, resulting in about 136.000 cells in total. Precursor simulation of the fully-developed channel flow ($Re_\tau \approx 290$) was performed in order to generate appropriate inflow. The interface development corresponds approximately to the one displayed in Fig. 4 with $y^+_{ifce} \approx 48$. The grid used by Avancha and Pletcher was of comparable size. The same solution domain was meshed by $72 \times 46 \times 48$ cells downstream of the step and $17 \times 31 \times 48$ cells upstream of the step resulting in about 184.000 cells in total.

RESULTS AND DISCUSSION

Some selected results obtained by the present near-wall, $\widetilde{\overline{\varrho} u''_i u''_j} - \varepsilon^h$ RANS model (denoted by RSM) and the hybrid LES/RANS model (denoted by HLR) for both the isothermal flow and the cases involving severe property variations due to the strong wall heating are shown and discussed in the next subsections along the reference experimental (Kasagi and Matsunaga, 1995) and reference LES (Avancha, 2001 and Avancha and Pletcher, 2002) database. In addition, the results obtained by the pure LES method using the SGS model of Smagorinsky and the same grid resolution as in the case of the HLR model scheme are also displayed. These "coarse" LES appropriate results are denoted by LESc.

Isothermal flow

The comparison of the mean streamline patterns in the recirculation region, Fig. 5, shows that the present hybrid LES/RANS schemes yields the reattachment length of $x_r/H = 6.9$, somewhat larger compared to the experimental one $x_r/H = 6.51$. A similar discrepancy applies also to the corner bubble. The same conclusion can be deduced from the friction factor shown in Fig. 6. In contrast, the result of Avancha (2001) indicates a zero C_f at $x_r/H \approx 5.4$ (though the reattachment length quoted explicitly was $x_r/H = 6.1$). It is difficult to judge the credibility of the latter finding in the absence of appropriate measurements (C_f evolution was not available in the experimental database of Kasagi and Matsunaga). Because of that, the results of some other experimental (Jovic and Driver, 1993) and computational studies (DNS: Le et al., 1997; LES: Saric et al., 2005) of the backward-facing step configurations at comparable flow Reynolds numbers (Re_H) and expansion ratios (ER) are also displayed in Fig. 6. The C_f-evolution obtained by the HLR model agrees reasonably with these results with respect to both the main and secondary reattachment lengths, in contrast to the LES results of Avancha and Pletcher, which report both lengths to be substantially shorter. Furthermore, the negative peak value is too high and the C_f-evolution in the recovery region indicates a significant underprediction. Also, these results show some curious behaviour immediately after expansion, such as high positive values at the separation point $x/H = 0$, where, per definition, C_f should take zero value.

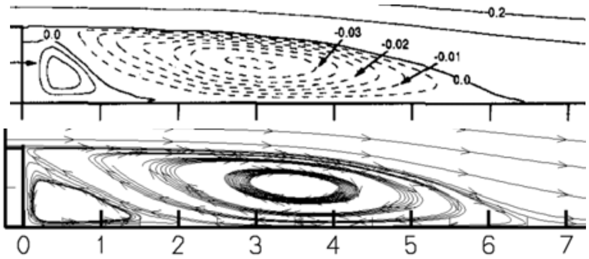

Figure 5: Mean streamlines obtained a) experimentally (upper) and applying the present HLR model (lower)

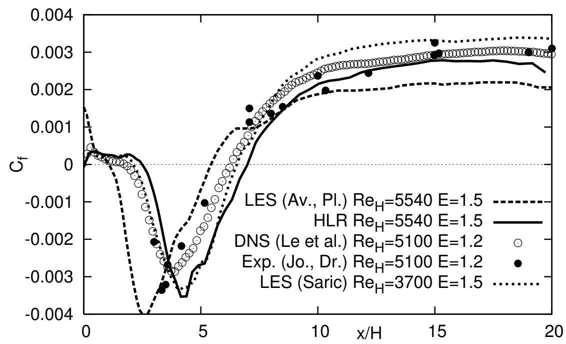

Figure 6: Friction coefficient evolution

Fig. 7 displays excellent agreement between present computational results and experimental data in all characteristic regions of the backward-facing step configuration.

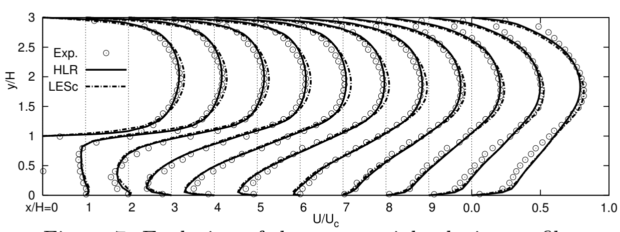

Figure 7: Evolution of the mean axial velocity profiles

Cases with wall heating

The simulations were performed for three different wall heat fluxes $q_w = 1$, 2 and $3\,kW/m^2$ (corresponding to the normalized heat flux levels - $Q_w = q_w/(\varrho_{ref} C_p U_{ref} T_{ref})$ - of 0.0014, 0.0028 and 0.0042). Fig. 8 depicts the mean axial velocity and mean temperature evolution for the case with the highest wall heat flux level $q_w = 3\,kW/m^2$. Direct comparison of the mean velocity field with the isothermal case (putting the profiles into the same diagram) reveals very weak influence of the strong temperature variation on the reattachment length (the same conclusion can be drawn from the C_f evolutions for all three heat flux levels, Fig. 9). Apart from a certain deviation between the model results

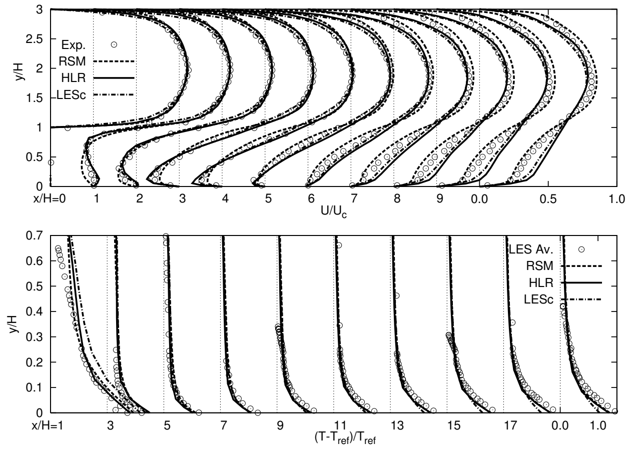

Figure 8: Evolution of the mean axial velocity and mean temperature profiles - $q_w = 3kW/m^2$

(HLR and RSM), the most important change compared to the isothermal case is visible in the region of the secondary recirculation and associated reattachment region. The influence of the strong temperature gradient (the wall temperature for the case with $q_w = 3\,kW/m^2$ takes here the values slightly below $1000\,K$, Figs. 10 and 11) on the flow immediatelly after expansion is visible in all following diagrams. The C_f evolutions displayed in Fig. 9 reveal a very

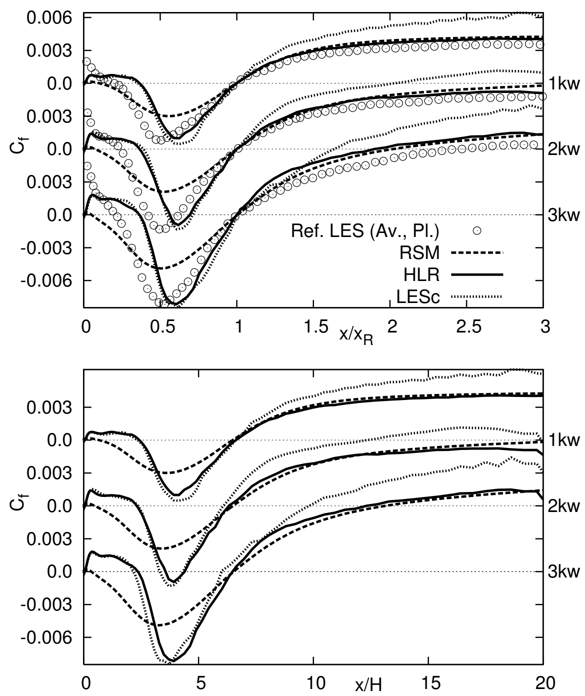

Figure 9: Friction coefficient evolution for all three cases with wall heating - $q_w = 1$, 2 and $3kW/m^2$

interesting dependence on the heat flux level supplied. In order to make direct comparison between the reference LES and the present computational results the values on x-axis are normalized with the corresponding reattachment length (see discussion about reattachment length predictions in the previous subsection). Both the negative peak in the recirculation zone (up to three times higher magnitude compared to the isothermal case; the RSM model underpredicts significantly the reference LES and the present HLR results) and the positive maximum value in the recovery region (an increase of 100% compared to the case with $q_w = 0$) increase with the heat flux level increase. Such an outcome is pertinent to the intensification of the convective mixing within the separation bubble due to the strong heating. Although less intensive, an analogous acceleration occurs in the immediate wall vicinity within recovery region. The C_f predictions obtained with the reference LES exhibit, similar as in the isothermal flow, unrealistic (high) final values at the fixed separation point $x = 0$. Both the bulk and the

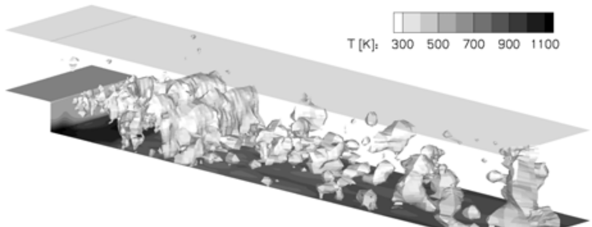

Figure 10: Contours of the fluctuating pressure coloured with the instantaneous temperature - $q_w = 3kW/m^2$

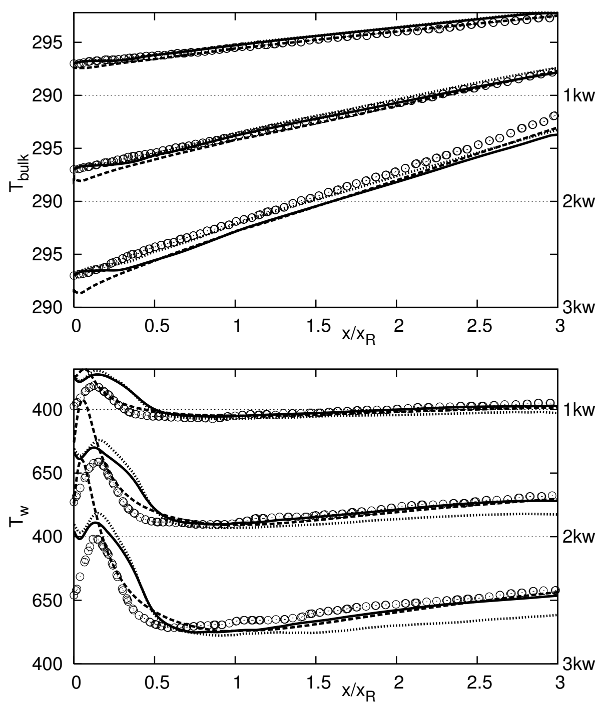

Figure 11: Bulk (upper) and wall (lower) temperature variation for all three cases with wall heating - $q_w = 1$, 2 and $3kW/m^2$

wall temperature variations agree very well with the reference LES. Fig. 12 displays the variation of the coefficient of the dynamic viscosity. As expected, $\overline{\mu}$ reaches its maximum at the position coinciding with the secondary reattachment location, where the backflow in the mean recirculation zone and the (positive) flow within the corner bubble hit each other. A direct comparison with the reference LES data in this region is inadequate because of the reasons explained previously. Both databases exhibit a high level of agreement in the recovery region. The evolution of Stanton number ($St = Q_w T_{ref}/(T_w - T_{bulk})$) depicted in Fig. 13 reflects entirely the bulk and wall temperature variations.

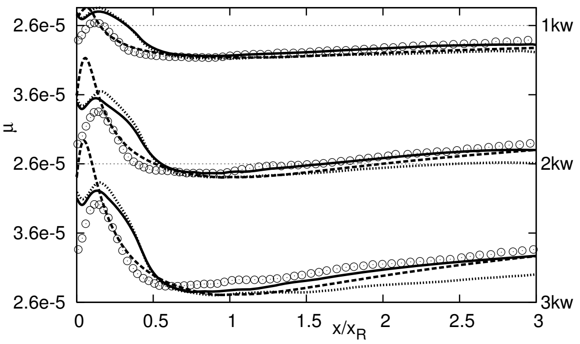

Figure 12: Variation of the viscosity for all three cases with wall heating - $q_w = 1$, 2 and $3kW/m^2$

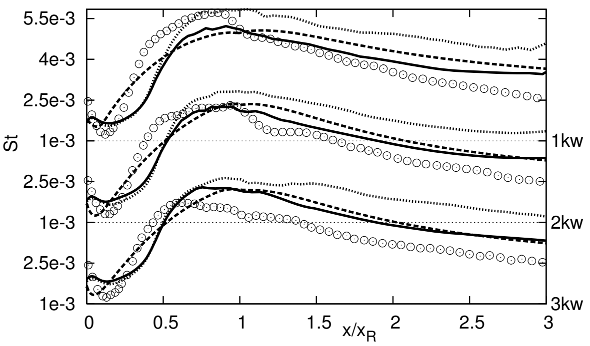

Figure 13: Stanton number variation for all three cases with wall heating - $q_w = 1$, 2 and $3kW/m^2$

No results corresponding to the turbulence field are shown due to the space limitation. It can only be said that the Reynolds stress components exhibit very weak dependence on the thermal field.

CONCLUSIONS

The capability of a newly proposed hybrid LES/RANS model scheme employing low-Reynolds number, eddy-viscosity-based RANS model in the near-wall layer and the Smagorinsky SGS model in the core flow was demonstrated by computing the separating flow behind a backward-facing step involving strong fluid property variation due to uniform heat flux supplied through the bottom wall downstream of the step. A variable interface between RANS and LES regions was applied, whose position was controlled by a parameter corresponding to an in-advance prescribed fraction of kinetic energy of turbulence. The RANS calculations with a near-wall, second-moment closure employing the homogeneous dissipation as the scale supplying variable were performed in parallel. The results obtained by both computational models (RSM and HLR) with respect to the reattachment lengths, C_f and Stanton number evolutions, fluid flow and thermal fields follow closely the reference experiment (Kasagi and Matsunaga, 1995) and reference LES (Avancha and Pletcher, 2002). This is especially the case in the recovery region. The deviations related to the wall temperature and flow property variations, concentrated mostly in the region of the corner bubble immeditelly after sudden expansion, are associated with the inadequate reference LES predictions (Avancha and Pletcher) of the secondary reattachment length. The HLR results are generally superior to the LES data obtained on the same grid.

Acknowledgements

The financial support of the Deutsche Forschungsgemeinschaft through the grant SFB568 "Flow and Combustion in Future Gas Turbine Combustion Chambers" for B. Kniesner and R. Jester-Zürker and the award of guest professorship from the German academic exchange service (DAAD) for K. Hanjalic are gratefully acknowledged.

REFERENCES

Avancha, R.V.R., 2001, "A study of the heat transfer and fluid mechanics of the turbulent separating and reattaching flow past a backward-facing step using large-eddy simulation", Ph.D. Thesis, Iowa State University

Avancha, R.V.R. and Pletcher, R.H., 2002, "Large eddy simulation of the turbulent flow past a backward-facing step with heat transfer and property variations", *Int. J. Heat and Fluid Flow*, Vol. 23, pp. 601-614

Chien, K.-Y., 1982, "Predictions of Channel and Boundary-Layer Flows with a Low-Reynolds-Number Turbulence Model", *AIAA Journal*, Vol. 20(1), pp. 33-38

Kasagi, N. and Matsunaga, A., 1995, "Three-dimensional particle-tracking velocimetry measurements of turbulence statistics and energy budget in a backward facing step flow", *Int. J. Heat and Fluid Flow*, Vol. 16, pp. 477-485

Jakirlic, S. and Hanjalic, K., 2002, "A new approach to modelling near-wall turbulence energy and stress dissipation", *J. Fluid Mech.*, Vol. 539, pp. 139-166

Jester-Zürker, R. and Jakirlic, S., 2005, "Heat transfer modelling in a channel flow with variable fluid properties accounting for near-wall turbulence", 4th International Conference on *Computational Heat and Mass Transfer*, Paris-Cachan, France, May 17-20

Jovic, S. and Driver, D., 1995, "Reynolds number effects on the skin friction in separated flows behind a backward-facing step", *Experiments in Fluids*, Vol. 18(6), pp. 464-467

Kniesner, B., Jakirlic, S. and Hanjalic, K., 2006, "Scrutinizing hybrid RANS/LES approaches in separating flows with heat transfer", *Conference on Modelling Fluid Flow* - CMFF'06, Budapest, Hungary, September 6-9

Lai, Y. G., and So, R. M. C., 1990, "Near-wall modelling of turbulent heat fluxes", *Int. J. Heat Mass Transfer*, Vol. 33(7), pp. 1429-1440

Le, H., Moin, P. and Kim, J., 1997, "Direct Numerical Simulation of Turbulent Flow over a Backward-Facing Step", *J. Fluid Mech.*, Vol. 330, pp. 349-374

Mason, P.J. and Callen, N.S., 1986, "On the magnitude of the subgrid-scale eddy coefficient in large-eddy simulation of turbulent channel flow", *J. Fluid Mech.*, Vol. 162

Saric, S., Jakirlic, S. and Tropea, C., 2005, "A periodically perturbed backward-facing step flow by means of LES, DES and T-RANS: an example of flow separation control", *ASME J. of Fluids Engineering*, Vol. 127, pp. 879-887

Seki, Y., Kawamoto, N., and Kawamura, H., 2003, "Proposal of turbulent heat flux model and its application to turbulent channel flow with various thermal boundary conditions", *Turbulence, Heat and Mass Transfer*, Vol. 4, Begell House Inc., pp. 569-576

Temmerman, L., Hadziabdic, M., Leschziner, M.A. and Hanjalic, K., 2005, "A hybrid two-layer URANS-LES approach for large eddy simulation at high Reynolds numbers", *Int. J. Heat Fluid Flow*, Vol. 26, pp. 173-190